

1 ***Supplementary Information for***

2

3 **Real Roles of FeOCl Nanosheets in Fenton Process**

4 Haohao Chen<sup>†,‡</sup>, Na Wen<sup>‡</sup>, Yingping Huang<sup>‡,\*</sup>, Qintian Peng<sup>‡</sup>, Houle Zhou<sup>‡</sup>, Yuqing Zhu<sup>†,‡</sup>, Hailin  
5 Tian<sup>†,‡</sup>, Xin Ying Kong,<sup>&</sup> Huaiyong Zhu<sup>§</sup>, and Liqun Ye<sup>†,‡,\*</sup>

6 <sup>†</sup> College of Materials and Chemical Engineering, Key Laboratory of Inorganic Nonmetallic  
7 Crystalline and Energy Conversion Materials, China Three Gorges University, Yichang 443002,  
8 Hubei, China.

9 <sup>‡</sup> Engineering Research Center of Eco-Environment in Three Gorges Reservoir Region, Ministry of  
10 Education, China Three Gorges University, Yichang 443002, Hubei, China.

11 <sup>&</sup> School of Chemistry, Chemical Engineering and Biotechnology, Nanyang Technological  
12 University, Singapore, 21 Nanyang Link, 637371 Singapore.

13 <sup>§</sup> School of Chemistry and Physics, Queensland University of Technology, Brisbane, QLD 4001,  
14 Australia.

15  
16 \* E-mail: chem\_ctgu@126.com (Y. Huang); lqye@ctgu.edu.cn (L. Ye)

17

18

19

20

21

22

23

24

25

26

27 27 Pages, 22 Figures, 1 Tables

28

29 **CONTENTS**

30 **1. Experimental Details**

31 **2. Figures**

32 **Figure S1.** XRD spectra of FeOCl calcined under different conditions including vacuum, fully open,  
33 and partially open glass flasks.

34 **Figure S2.** SEM image of FeOCl calcined in a crucible.

35 **Figure S3.** Survey XPS spectrum of FeOCl fabricated in glass flasks.

36 **Figure S4.** HPLC chromatograms (a) and calibration curve (b) of different concentrations of  
37 hydrogen peroxide. HPLC chromatograms of ATZ different concentrations (c) and its respective  
38 calibration curve (d).

39 **Figure S5.** Adsorption-desorption equilibrium of FeOCl with 5% adsorption.  $[\text{FeOCl}] = 200 \text{ mg/L}$ ,  
40  $[\text{ATZ}] = 0.5 \text{ mg/L}$ .

41 **Figure S6.** HPLC chromatograms of  $\text{H}_2\text{O}_2/\text{ATZ}$  system (a) and  $\text{H}_2\text{O}_2/\text{ATZ}/\text{light}$  system (b).

42 **Figure S7.** The plot of temperature variation in different catalytic systems (a). The plot of dissolved  
43 oxygen variation in different catalytic systems (b).

44 **Figure S8.** Effect of 500 mM methanol ( $\cdot\text{OH}$  scavenger) on ATZ degradation, where  $[\text{MeOH}] =$   
45  $500 \text{ mM}$ ,  $[\text{H}_2\text{O}_2] = 5 \text{ mM}$ ,  $[\text{FeOCl}] = 200 \text{ mg/L}$ ,  $[\text{ATZ}] = 0.5 \text{ mg/L}$ .

46 **Figure S9.** Calibration curves for different concentrations of 2-hydroxyterephthalic acid (a).  
47 First-order kinetic fitting curves of  $\cdot\text{OH}$  concentration in different catalytic systems (b).  
48 Fluorescence spectra of FeOCl/ $\text{H}_2\text{O}_2$ /light system (c) and FeOCl/ $\text{H}_2\text{O}_2$  system (d) after adding TA.  
49  $[\text{TA}] = 5 \text{ mM}$ ,  $[\text{H}_2\text{O}_2] = 5 \text{ mM}$ ,  $[\text{FeOCl}] = 200 \text{ mg/L}$ .

50 **Figure S10.** Removal rates of NBT in different catalytic systems (a) and standard curve of different  
51 concentrations of NBT(b).  $[\text{NBT}] = 24 \text{ }\mu\text{M}$ ,  $[\text{H}_2\text{O}_2] = 5 \text{ mM}$ ,  $[\text{FeOCl}] = 200 \text{ mg/L}$ ,  $[\text{ATZ}] = 0.5$   
52  $\text{mg/L}$ .

53 **Figure S11.** HPLC chromatograms of FFA consumption by FeOCl/ $\text{H}_2\text{O}_2$ /light system (a) and  
54 FeOCl/ $\text{H}_2\text{O}_2$  system (b). FFA removal rates in different catalytic systems (c) and standard curve of  
55 FFA at different concentrations (d).  $[\text{FFA}] = 40 \text{ }\mu\text{M}$ ,  $[\text{H}_2\text{O}_2] = 5 \text{ mM}$ ,  $[\text{FeOCl}] = 200 \text{ mg}$ .

56 **Figure S12.** The quantitative relationships between  $\cdot\text{OH}$ ,  $\text{O}_2^{\cdot-}$ , and  $^1\text{O}_2$  in different catalytic  
57 systems.

58 **Figure S13.** PMSO consumption and PMSO<sub>2</sub> generation in FeOCl/H<sub>2</sub>O<sub>2</sub>/light system (a). PMSO  
59 consumption and PMSO<sub>2</sub> generation in the FeOCl/H<sub>2</sub>O<sub>2</sub> system (b). HPLC chromatograms and  
60 calibration curves of different gradient concentrations of PMSO (c-d) and PMSO<sub>2</sub> (e-f),  
61 respectively.

62 **Figure S14.** Total iron dissolution before reaction and ATZ removal after 2h of reaction at different  
63 initial pH in FeOCl/H<sub>2</sub>O<sub>2</sub>/light systems (a). pH change after 2h reaction at different initial pH In  
64 FeOCl/H<sub>2</sub>O<sub>2</sub>/light system. [H<sub>2</sub>O<sub>2</sub>] = 5 mM, [FeOCl] = 200 mg/L, [ATZ] = 0.5 mg/L.

65 **Figure S15.** Removal of ATZ by trace iron. [H<sub>2</sub>O<sub>2</sub>] = 5 mM, [FeOCl] = 200 mg/L, [ATZ] = 0.5  
66 mg/L.

67 **Figure S16.** First-order kinetic fitting curves for the removal of atrazine by trace iron ions.

68 **Figure S17.** Cyclic experiments with FeOCl and dissolved iron for ATZ removal. [H<sub>2</sub>O<sub>2</sub>] = 5 mM,  
69 [ATZ] = 0.5 mg/L, pH = 4.

70 **Figure S18.** Calibration curve for different concentrations of iron.

71 **Figure S19.** Calibration curve for different concentrations of Cl<sup>-</sup> (a). IC chromatogram of Cl<sup>-</sup> at  
72 different concentrations of FeOCl in FeOCl/H<sub>2</sub>O system at 200 min (b). Concentration of chlorine  
73 ions in different catalytic systems (c). [H<sub>2</sub>O<sub>2</sub>] = 5 mM, [FeOCl] = 200 mg/L, [ATZ] = 0.5 mg/L.

74 **Figure S20.** PH changes in different systems (a). XRD spectra of fresh and used FeOCl in  
75 FeOC/H<sub>2</sub>O<sub>2</sub>/ATZ/light system (b). [H<sub>2</sub>O<sub>2</sub>] = 5 mM, [FeOCl] = 200 mg/L, [ATZ] = 0.5 mg/L.

76 **Figure S21.** SEM image of FeOCl after one month storage.

77 **Figure S22.** ESI(+)-MS to detect the products from ATZ degradation. Degradation of ATZ over  
78 FeOCl/H<sub>2</sub>O<sub>2</sub>/light system after 30 min (b), 60 min (c), and 120 min (d) of reaction. Degradation of  
79 ATZ over FeOCl/H<sub>2</sub>O<sub>2</sub> system after 60 min (e) and 120 min (f) of reaction.

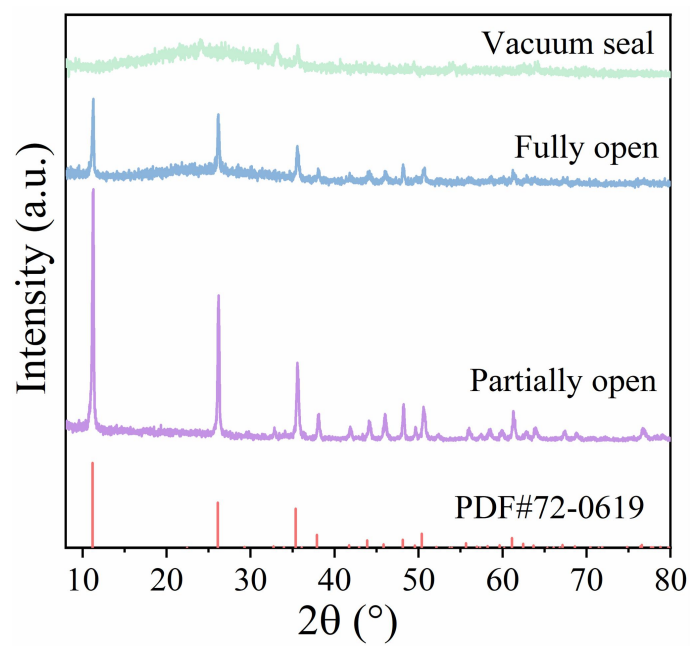
80

81 **1. Experimental Details**

82 **1.1. Materials.** All chemical reagents including tert-butyl alcohol (TBA) and ethanol (EtOH)  
83 are of analytical purity. Terephthalic acid (TA), p-nitro blue chloride (NBT), glacial acetic acid, and  
84 atrazine were purchased from Aladdin Chemical Company, China. Ferric chloride hexahydrate and  
85 ferrous sulfate were purchased from Shanghai Maclean Biochemical Technology Co. The 30%  
86 hydrogen peroxide and sodium acetate were purchased from Xilong Science Co. Chromatography  
87 grade methanol and acetonitrile were purchased from American Skyland Co. o-Diazophenanthrene  
88 was purchased from Shanghai Hao Hong Biopharmaceutical Co whereas sodium hydroxide was  
89 purchased from Tianjin Comio Chemical Reagent Co.

90 **1.2. Materials characterization.** The X-ray diffraction (XRD) pattern of FeOCl was  
91 characterized using a Bruker D8 advanced  $K_{\alpha}$  X-ray diffractometer with a  $2\theta$  scan rate of  $5^{\circ} \text{ min}^{-1}$ .  
92 The FeOCl surface elemental species and valence states were determined using a Thermos  
93 ESCALAB 250Xi XPS instrument (Al  $K_{\alpha}$ , 150 W, C 1 s 284.6 eV). The surface morphology of  
94 FeOCl was analyzed by JSM-7500F emission scanning electron microscope (SEM), Tecnai G2 F30  
95 transmission electron microscope (TEM), and elemental mapping from Nippon Electron  
96 Corporation.

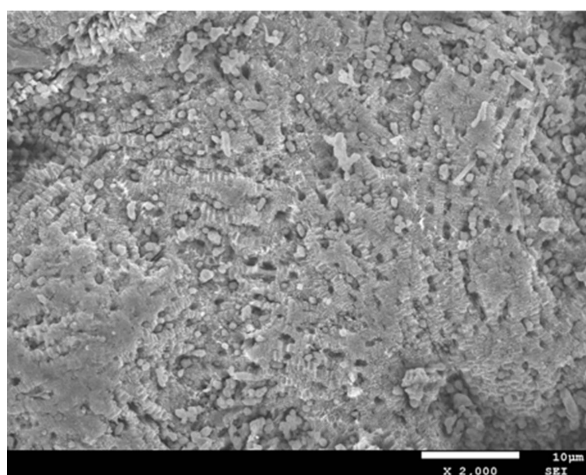
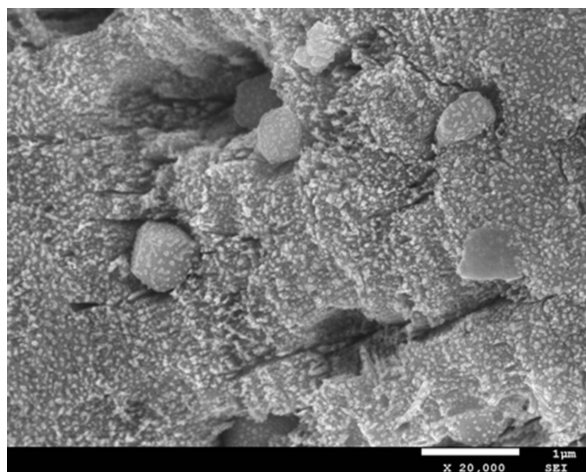
97



98

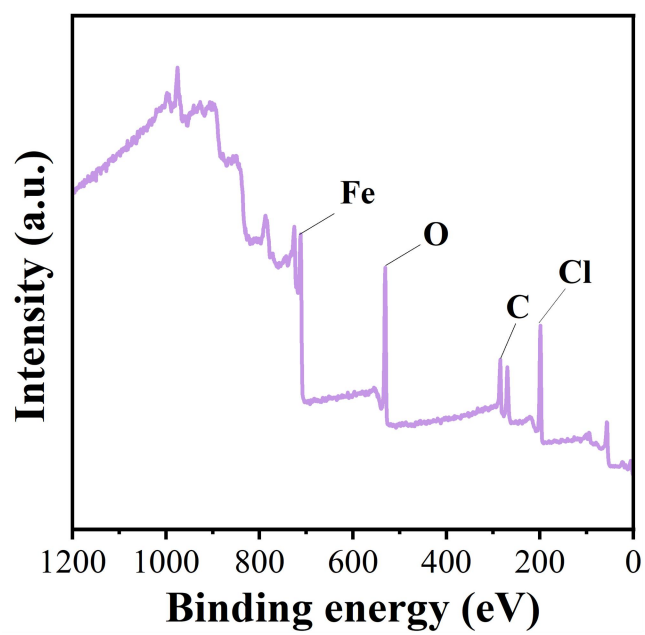
99 **Figure S1.** XRD spectra of FeOCl calcined under different conditions including vacuum, fully open,  
100 and partially open glass flasks.

101



102  
103  
104

**Figure S2.** SEM image of FeOCl calcined in a crucible.

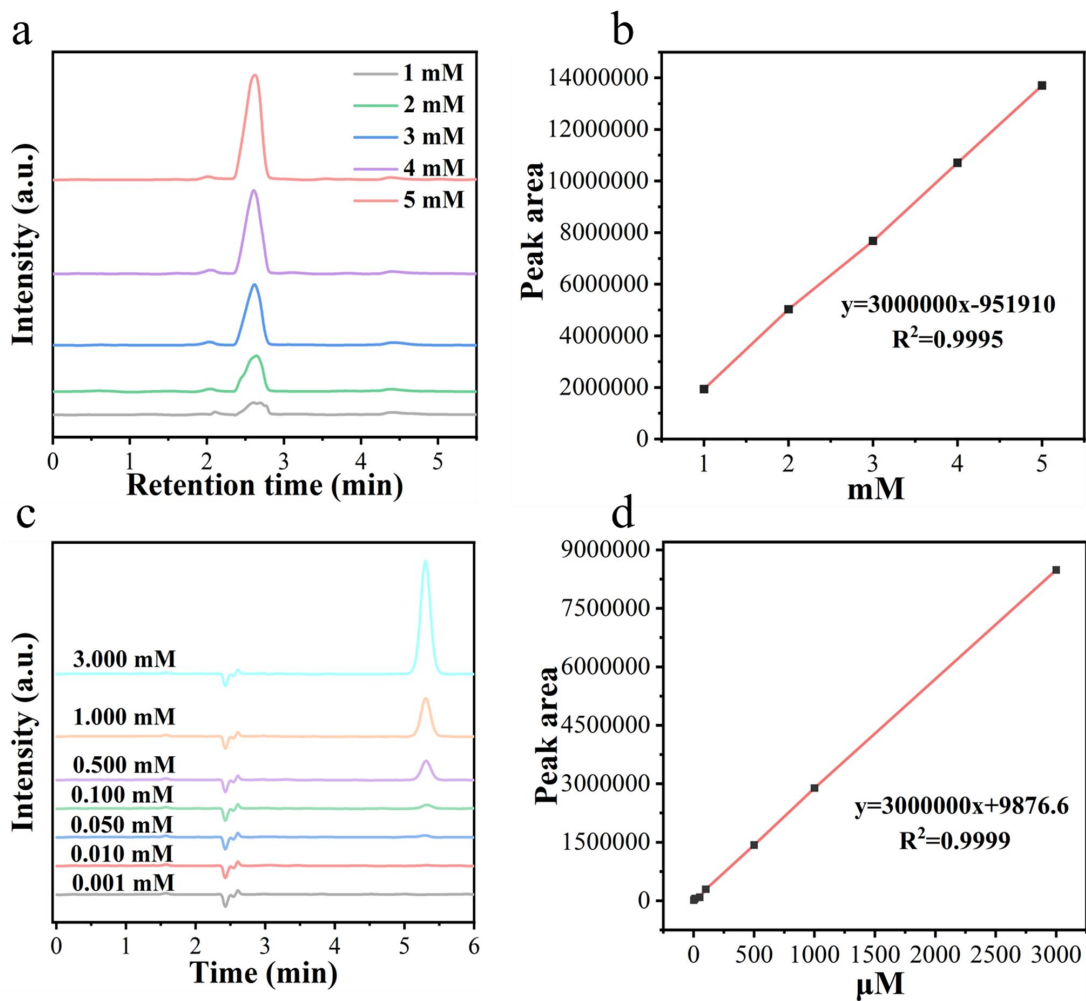


105

106

**Figure S3.** Survey XPS spectrum of FeOCl fabricated in glass flasks.

107

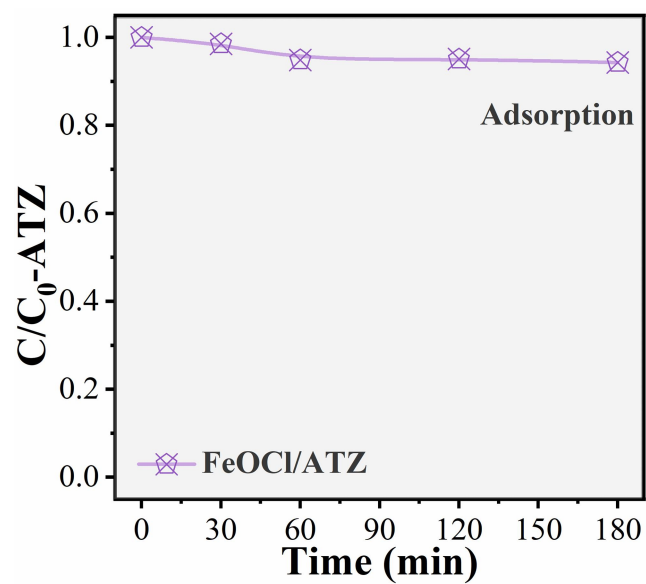


108

109 **Figure S4.** HPLC chromatograms (a) and calibration curve (b) of different concentrations of  
 110 hydrogen peroxide. HPLC chromatograms of ATZ different concentrations (c) and its respective  
 111 calibration curve (d).

112

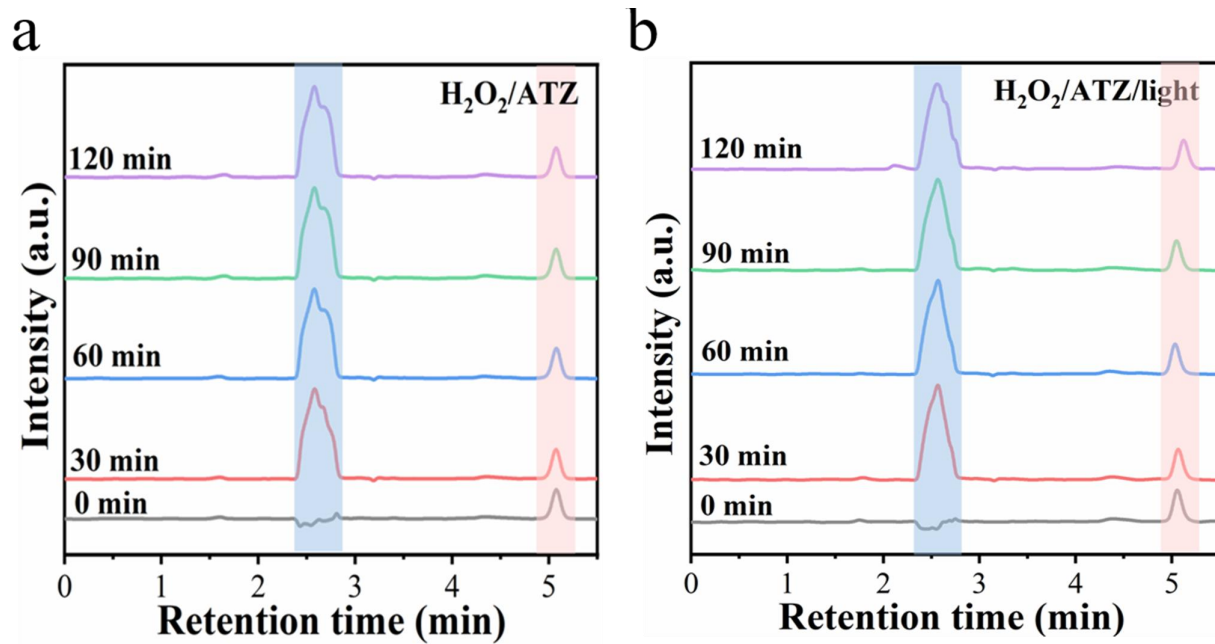




113

114 **Figure S5.** Adsorption-desorption equilibrium of FeOCl with 5% adsorption. [FeOCl] = 200 mg/L,  
115 [ATZ] = 0.5 mg/L.

116

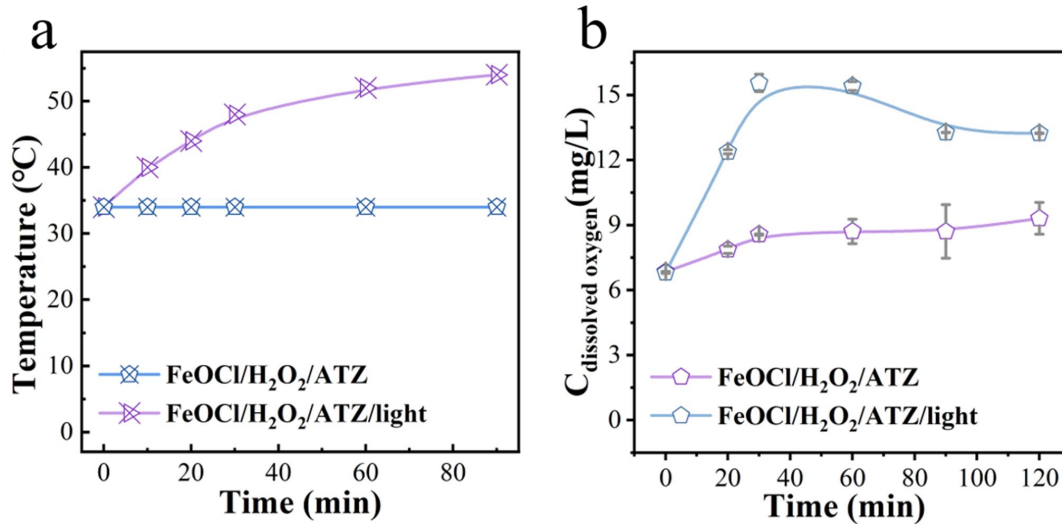


117

118

**Figure S6.** HPLC chromatograms of H<sub>2</sub>O<sub>2</sub>/ATZ system (a) and H<sub>2</sub>O<sub>2</sub>/ATZ/light system (b).

119

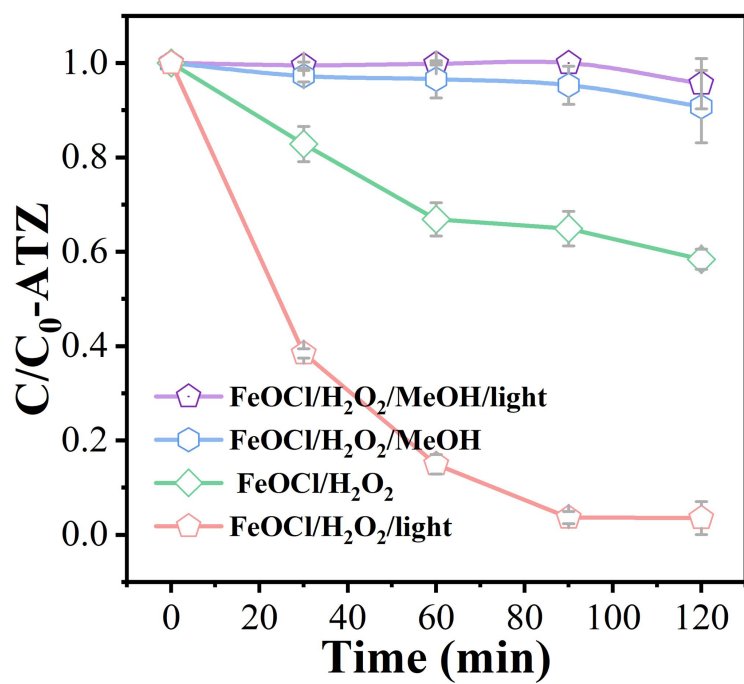


120

121 **Figure S7.** The plot of temperature variation in different catalytic systems (a). The plot of dissolved

122 oxygen variation in different catalytic systems (b).

123

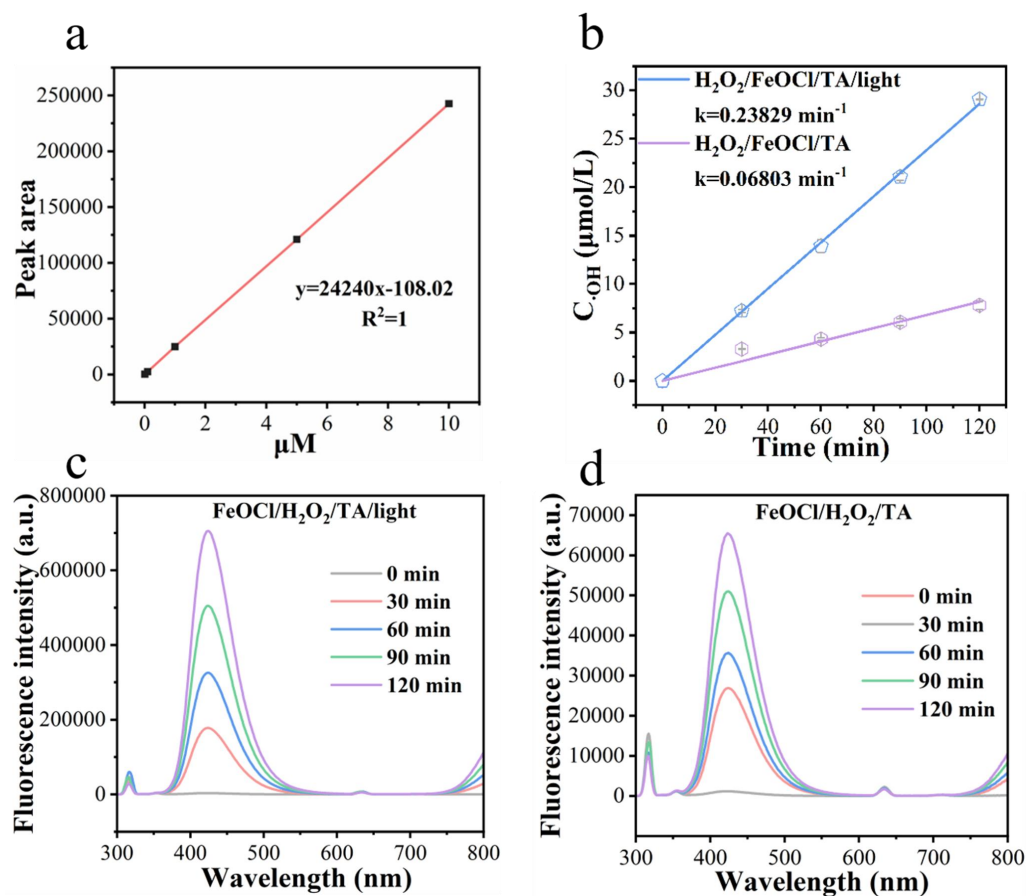


124

125 **Figure S8.** Effect of 500 mM methanol ( $\bullet$ OH scavenger) on ATZ degradation, where [MeOH] =

126 500 mM, [H<sub>2</sub>O<sub>2</sub>] = 5 mM, [FeOCl] = 200 mg/L, [ATZ] = 0.5 mg/L.

127



128

129 **Figure S9.** Calibration curves for different concentrations of 2-hydroxyterephthalic acid (a).

130 First-order kinetic fitting curves of  $\cdot\text{OH}$  concentration in different catalytic systems (b).

131 Fluorescence spectra of FeOCl/H<sub>2</sub>O<sub>2</sub>/light system (c) and FeOCl/H<sub>2</sub>O<sub>2</sub> system (d) after adding TA.

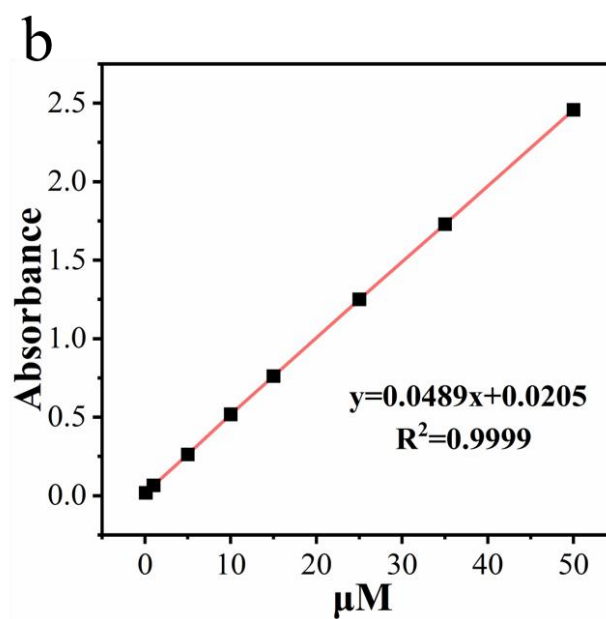
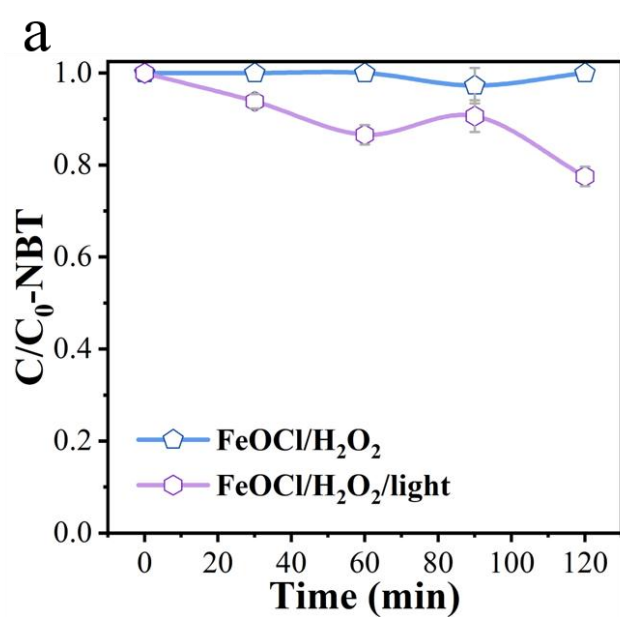
132 [TA] = 5 mM, [H<sub>2</sub>O<sub>2</sub>] = 5 mM, [FeOCl] = 200 mg/L.

133 Comparison of the amount of hydroxyl radicals produced by the photo-Fenton process and the

134 Fenton process:

$$r = \frac{k (H_2O_2/FeOCl/TA/light)}{k (H_2O_2/FeOCl/TA)}$$

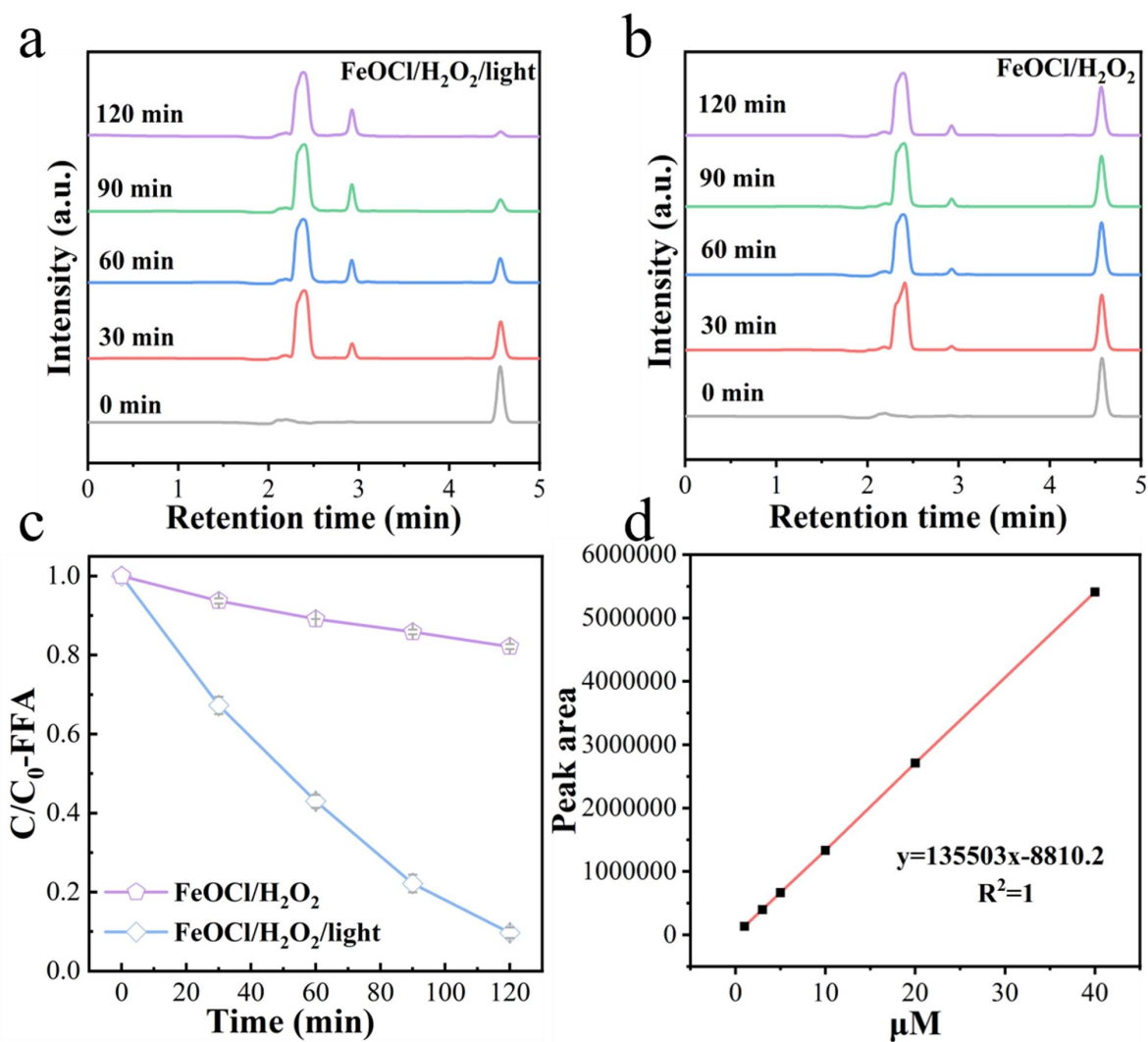
135



136

137 **Figure S10.** Removal rates of NBT in different catalytic systems (a) and standard curve of different  
 138 concentrations of NBT(b).  $[\text{NBT}] = 24 \mu\text{M}$ ,  $[\text{H}_2\text{O}_2] = 5 \text{ mM}$ ,  $[\text{FeOCl}] = 200 \text{ mg/L}$ ,  $[\text{ATZ}] = 0.5$   
 139  $\text{mg/L}$ .

140



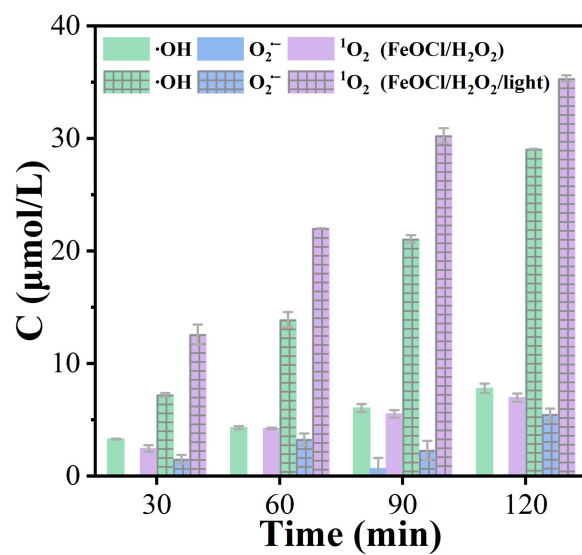
141

142 **Figure S11.** HPLC chromatograms of FFA consumption by FeOCl/H<sub>2</sub>O<sub>2</sub>/light system (a) and

143 FeOCl/H<sub>2</sub>O<sub>2</sub> system (b). FFA removal rates in different catalytic systems (c) and standard curve of

144 FFA at different concentrations (d). [FFA]= 40  $\mu\text{M}$ , [H<sub>2</sub>O<sub>2</sub>] = 5 mM, [FeOCl] = 200 mg.

145

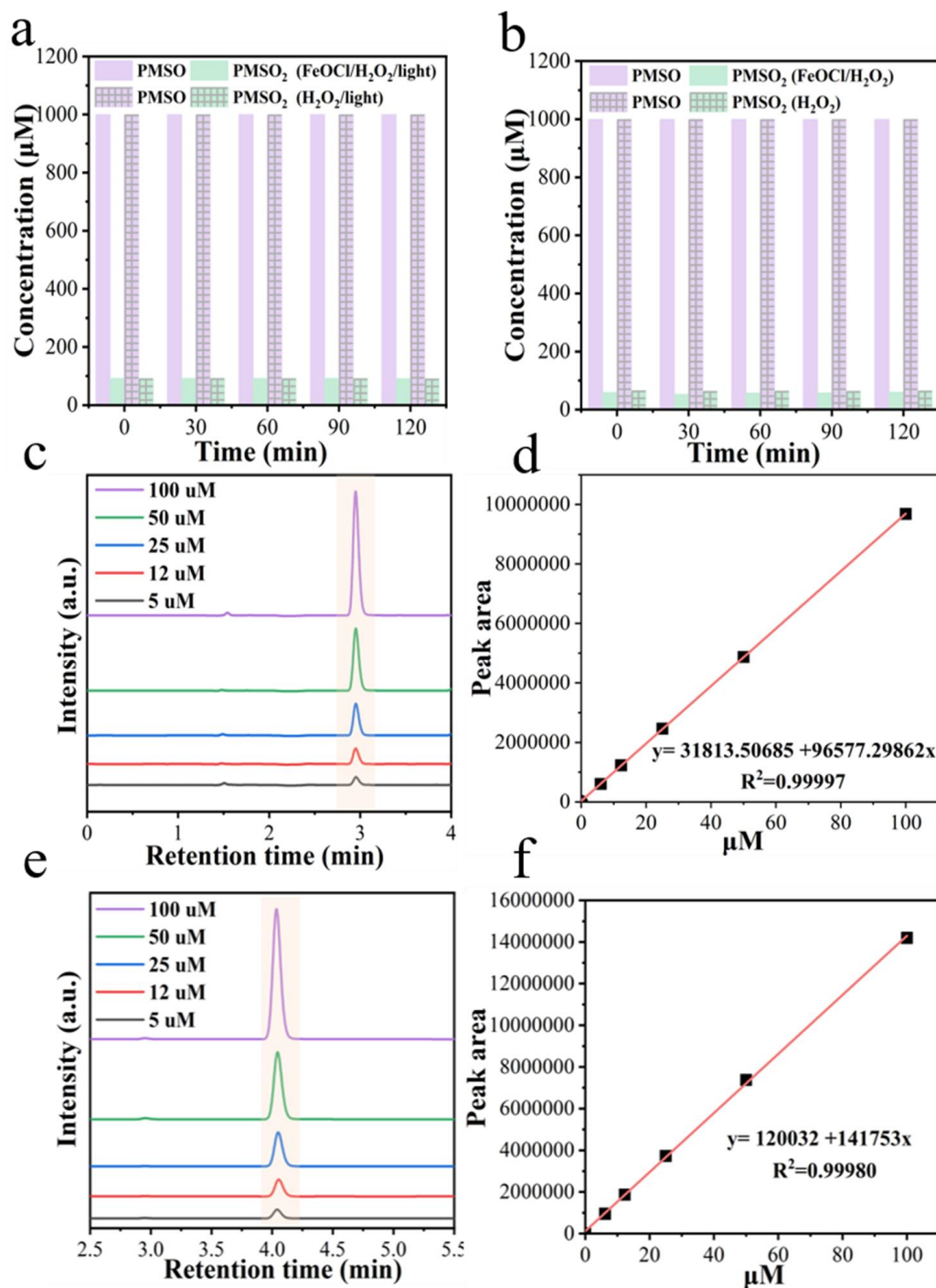


146

147 **Figure S12.** The quantitative relationships between  $\bullet\text{OH}$ ,  $\text{O}_2^{\bullet-}$ , and  $^1\text{O}_2$  in different catalytic  
 148 systems.

149

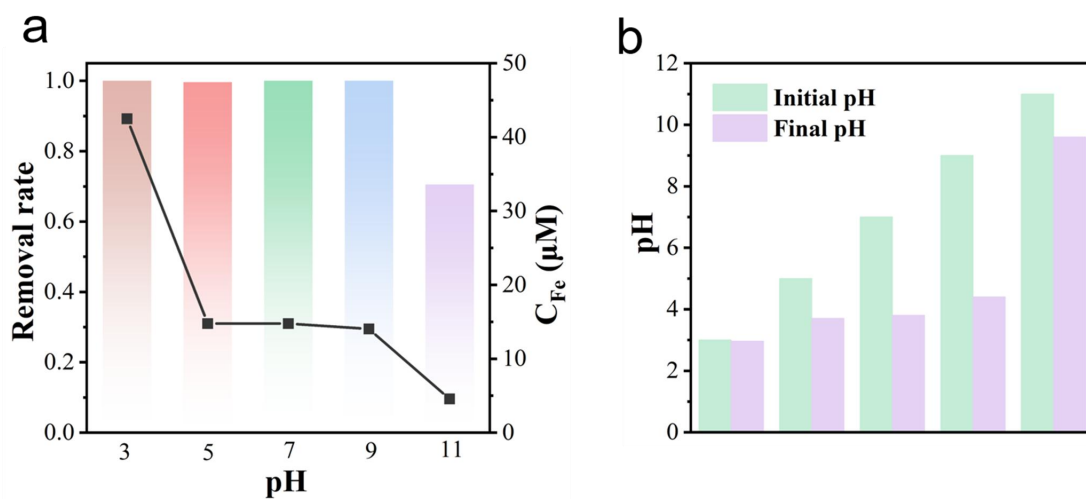




150

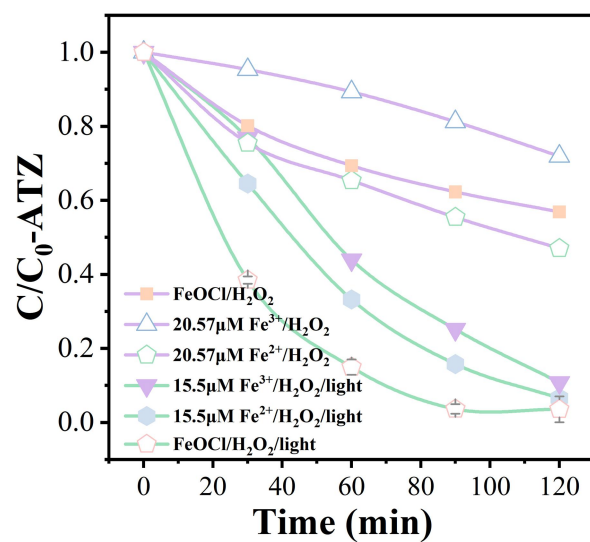
151 **Figure S13.** PMSO consumption and PMSO<sub>2</sub> generation in FeOCl/H<sub>2</sub>O<sub>2</sub>/light system (a). PMSO  
 152 consumption and PMSO<sub>2</sub> generation in the FeOCl/H<sub>2</sub>O<sub>2</sub> system (b). HPLC chromatograms and  
 153 calibration curves of different gradient concentrations of PMSO (c-d) and PMSO<sub>2</sub> (e-f),  
 154 respectively.

155



156

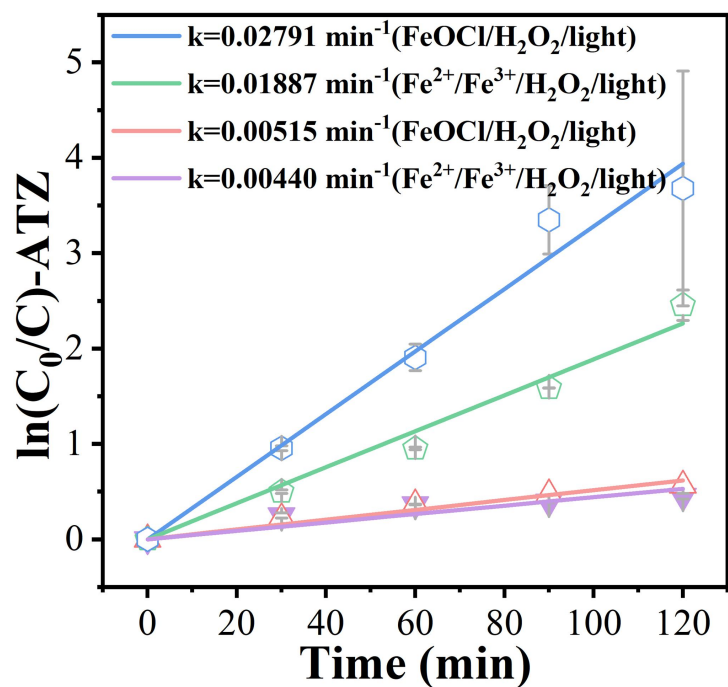
157 **Figure S14.** Total iron dissolution before reaction and ATZ removal after 2h of reaction at different  
 158 initial pH in FeOCl/H<sub>2</sub>O<sub>2</sub>/light systems (a). pH change after 2h reaction at different initial pH In  
 159 FeOCl/H<sub>2</sub>O<sub>2</sub>/light system. [H<sub>2</sub>O<sub>2</sub>] = 5 mM, [FeOCl] = 200 mg/L, [ATZ] = 0.5 mg/L.



161

162 **Figure S15.** Removal of ATZ by trace iron. [H<sub>2</sub>O<sub>2</sub>] = 5 mM, [FeOCl] = 200 mg/L, [ATZ] = 0.5

163 mg/L.



165

166 **Figure S16.** First-order kinetic fitting curves for the removal of atrazine by trace iron ions.

167 Homogeneous reaction, heterogeneous reaction percentage calculation method:

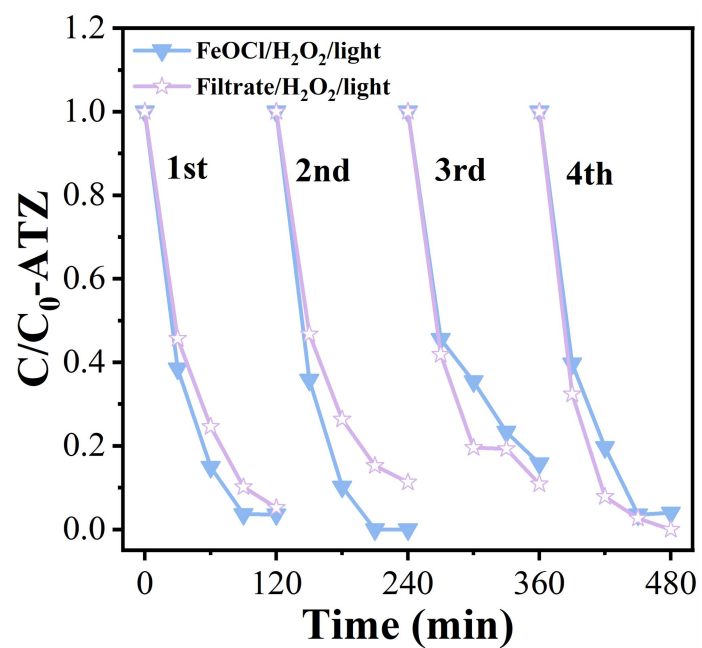
168 For FeOCl/H<sub>2</sub>O<sub>2</sub> systems:

$$\eta[\text{homogeneous reaction}] = \frac{k(\text{Fe}^{2+}/\text{Fe}^{3+}/\text{H}_2\text{O}_2)}{k(\text{FeOCl}/\text{H}_2\text{O}_2)}$$

169 For FeOCl/H<sub>2</sub>O<sub>2</sub>/light systems:

$$\eta[\text{heterogeneous reaction}] = \frac{k(\text{Fe}^{2+}/\text{Fe}^{3+}/\text{H}_2\text{O}_2/\text{light})}{k(\text{FeOCl}/\text{H}_2\text{O}_2/\text{light})}$$

170



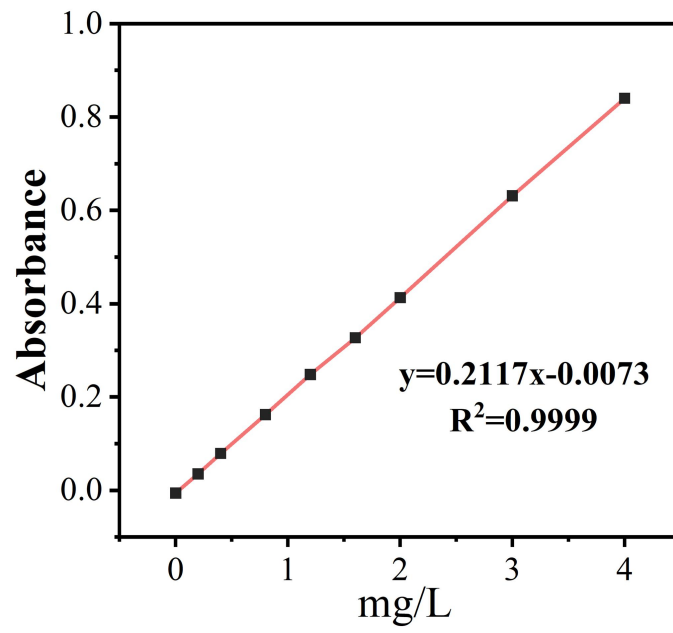
171

172 **Figure S17.** Cyclic experiments with FeOCl and dissolved iron for ATZ removal. [H<sub>2</sub>O<sub>2</sub>] = 5 mM,

173 [ATZ] = 0.5 mg/L, pH = 4.

174

175

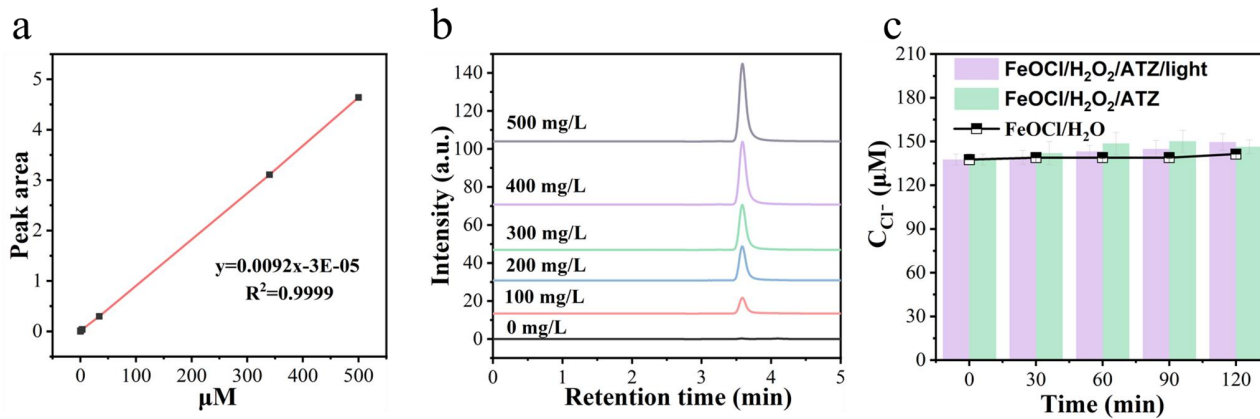


176

177

**Figure S18.** Calibration curve for different concentrations of iron.

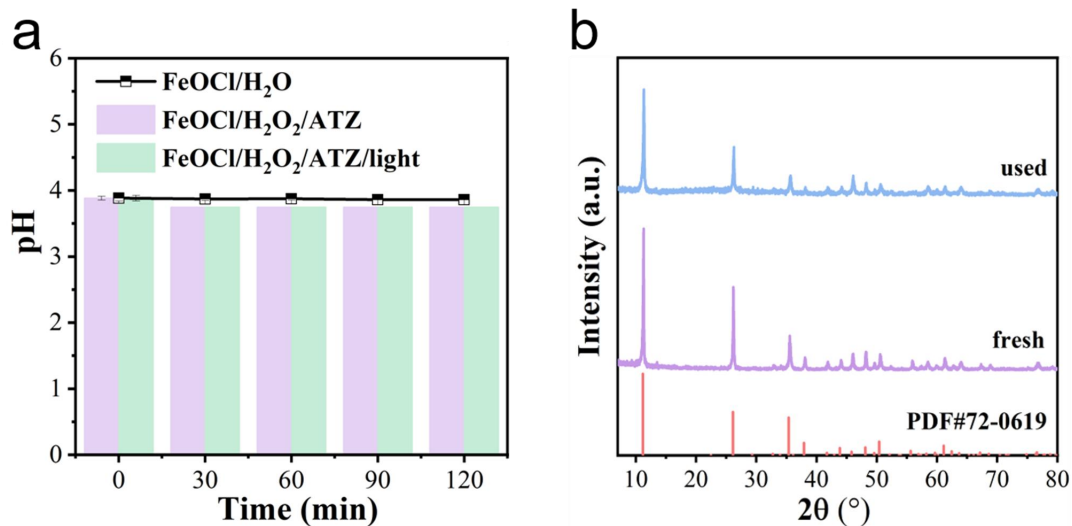
178



179

180 **Figure S19.** Calibration curve for different concentrations of  $\text{Cl}^-$  (a). IC chromatogram of  $\text{Cl}^-$  at  
 181 different concentrations of FeOCl in FeOCl/ $\text{H}_2\text{O}$  system at 200 min (b). Concentration of chlorine  
 182 ions in different catalytic systems (c).  $[\text{H}_2\text{O}_2] = 5 \text{ mM}$ ,  $[\text{FeOCl}] = 200 \text{ mg/L}$ ,  $[\text{ATZ}] = 0.5 \text{ mg/L}$ .

183



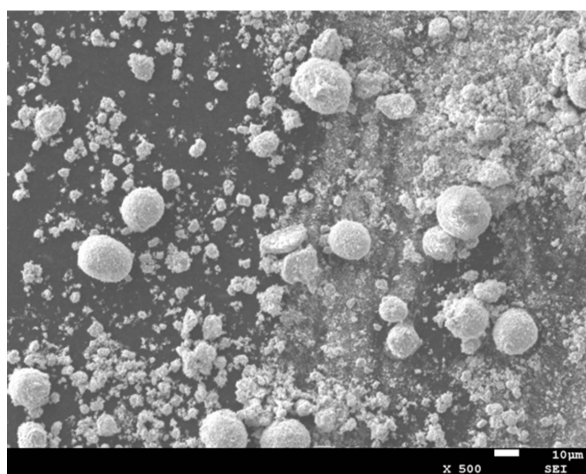
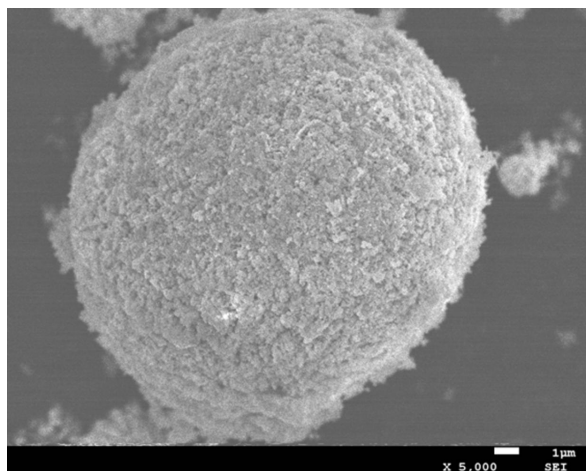
184

185 **Figure S20.** PH changes in different systems (a). XRD spectra of fresh and used FeOCl in

186 FeOC/H<sub>2</sub>O<sub>2</sub>/ATZ/light system (b). [H<sub>2</sub>O<sub>2</sub>] = 5 mM, [FeOCl] = 200 mg/L, [ATZ] = 0.5 mg/L.



187

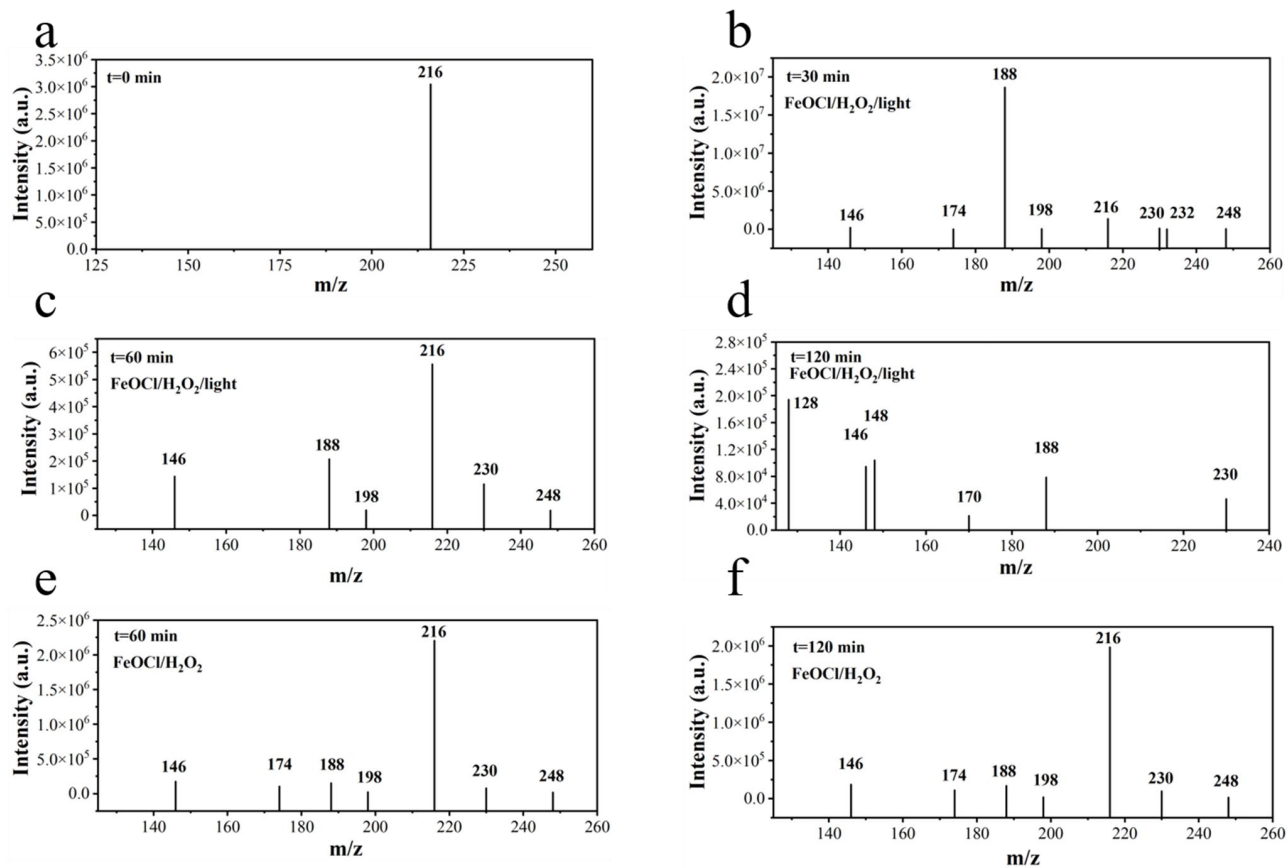


188

189

**Figure S21.** SEM image of FeOCl after one month storage.

190

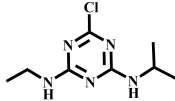
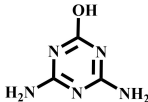
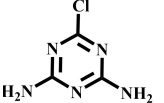
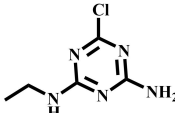
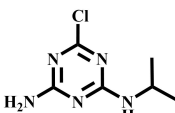
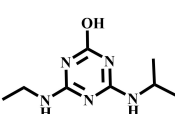
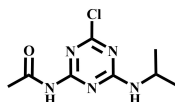
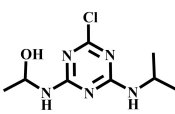
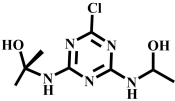


191

192 **Figure S22.** ESI(+)-MS to detect the products from ATZ degradation. Degradation of ATZ over  
 193 FeOCl/H<sub>2</sub>O<sub>2</sub>/light system after 30 min (b), 60 min (c), and 120 min (d) of reaction. Degradation of  
 194 ATZ over FeOCl/H<sub>2</sub>O<sub>2</sub> system after 60 min (e) and 120 min (f) of reaction.

195

196 **Table S1.** Intermediate products from ATZ degradation over FeOCl/H<sub>2</sub>O<sub>2</sub>/light system and  
 197 FeOCl/H<sub>2</sub>O<sub>2</sub> system.

Description	Molecular formula	Structural formula	Exact Mass	[M+H] <sup>+</sup>
ATZ	C <sub>8</sub> H <sub>14</sub> N <sub>5</sub> Cl		215.09	216.10
4,6-diamino-1,3,5-triazin-2-ol	C <sub>3</sub> H <sub>5</sub> N <sub>5</sub> O		127.05	128.05
6-chloro-1,3,5-triazine-2,4-diamine	C <sub>3</sub> H <sub>4</sub> N <sub>5</sub> Cl		145.02	146.02
6-chloro-N <sup>2</sup> -ethyl-1,3,5-triazine-2,4-diamine	C <sub>5</sub> H <sub>8</sub> N <sub>5</sub> Cl		173.05	174.05
6-chloro-N <sup>2</sup> -isopropyl-1,3,5-triazine-2,4-diamine	C <sub>6</sub> H <sub>10</sub> N <sub>5</sub> Cl		187.06	188.06
4-(ethylamino)-6-(isopropylamino)-1,3,5-triazin-2-ol	C <sub>8</sub> H <sub>5</sub> N <sub>5</sub> O		197.13	198.13
N-(4-chloro-6-(isopropylamino)-1,3,5-triazin-2-yl)acetamide	C <sub>8</sub> H <sub>12</sub> N <sub>5</sub> ClO		229.07	230.08
1-((4-chloro-6-(isopropylamino)-1,3,5-triazin-2-yl)amino)ethan-1-ol	C <sub>8</sub> H <sub>14</sub> N <sub>5</sub> ClO		231.09	232.09
2-((4-chloro-6-(1-hydroxyethyl)amino)-1,3,5-triazin-2-yl)amino)propan-2-ol	C <sub>8</sub> H <sub>14</sub> N <sub>5</sub> ClO <sub>2</sub>		247.08	248.09

198